Journal of Materials Chemistry C

PAPER

View Article Online
View Journal | View Issue

Cite this: J. Mater. Chem. C, 2014, 2, 3303

Uniaxial macroscopic alignment of conjugated polymer systems by directional crystallization during blade coating†

Bernhard Dörling,*[a] Varun Vohra,[b] Toan Thanh Dao,[b] Miquel Garriga,[a] Hideyuki Murata[b] and Mariano Campoy-Quiles*[a]

Received 17th October 2013
Accepted 25th November 2013

DOI: 10.1039/c3tc32056a

www.rsc.org/MaterialsC

We have developed a one step method for the deposition of uniaxially aligned conjugated polymer layers by directional epitaxial crystallization directly from solution. Oriented, square centimeter sized samples of poly(3-hexylthiophene) (P3HT) deposited from a chlorobenzene (CB) solution containing the additional crystallizable solvent 1,3,5-trichlorobenzene (TCB) are obtained by blade coating. Moreover, we show that the developed technique is not restricted to this specific material combination, but is instead applicable to a range of conjugated polymers and crystallizable solvents. Finally, we demonstrate the potential of this technique by realizing an organic photovoltaic device that exhibits a polarization dependent photoresponse.

Introduction

Conjugated polymers continue to be of interest due to their potential as a low-cost alternative to traditional semiconductor components in a range of applications. Uniaxial orientation of conjugated polymers allows us to perform fundamental studies on these systems as well as to develop new types of applications. On the one hand, orientation of the polymer chains along one direction has been employed to understand inter- and intra-chain transport in these materials.[1,2] Interestingly, orientation increases charge mobility even along the direction perpendicular to the preferred orientation axis.[2] Uniaxial orientation has also been employed to understand the optical properties of conjugated polymers, including the measurement of the angle between the polymer chain and the dipole moment,[3] the anisotropy upper limit[4] or the polarization dependence of the charge transfer state formed between a polymer and a fullerene.[5] On the other hand, novel types of devices can be created using oriented films, including polymer light emitting diodes (LEDs) with polarized emission,[6] organic photovoltaic (OPV) devices that show a polarization dependent photoresponse[7] and hidden security features only visible with polarized illumination.[8]

Over the past two decades, a multitude of methods have been developed for uniaxial orientation of polymers. These include mechanical stretching of the polymer layer,[8–11] annealing in the liquid crystal phase,[1,4,6] imprinting,[12] the use of rubbed templates[13] and direct rubbing of the polymer layer.[7,14,15]

Epitaxial growth of polymers on crystal templates is especially interesting, as it is potentially applicable to a wide range of materials.[16,17] For this method, like for those already mentioned, processing samples requires both multiple and complex steps, in this case applying a controlled lateral temperature gradient and subsequently removing a cover layer which is needed during processing. This makes their adaptation to large area devices unlikely.

A desirable implementation – one that is as simple as possible – would be one that works directly from solution. In an earlier report we demonstrated that epitaxial growth and the increased crystallinity that it entails can be achieved during spin coating from solution.[18] This is accomplished by co-depositing a crystallizable solvent together with the main solution. As the carrier solvent evaporates, the crystallizable solvent solidifies into large spherulites, which then serve as templates for the controlled growth of the solid species. As an added benefit, an increase in crystallinity, comparable to what would normally be obtained after an additional post-deposition annealing step, is observed.

In this work we explore further this orient-during-deposition concept by developing a method to deposit uniaxially aligned polymer layers with a fibrillar texture directly from solution *via* blade coating. A judicious control of the solvent compositions, the blade parameters, and the wet film drying kinetics enables us to fabricate films exhibiting orientation across several square centimeters. Using these fibrous layers, we demonstrate polymer:fullerene bilayer solar cells that exhibit a dichroic photoresponse greater than 2. Finally, we show that this method can

[a]Institut de Ciència de Materials de Barcelona (ICMAB-CSIC), Campus de la UAB, 08193 Bellaterra, Spain. E-mail: bdorling@icmab.es; mcampoy@icmab.es
[b]School of Materials Science, Japan Advanced Institute of Science and Technology (JAIST), Asahidai 1-1, Nomi, Ishikawa 923-1292, Japan

† Electronic supplementary information (ESI) available. See DOI: 10.1039/c3tc32056a

be extended to other crystallizable solvents and carrier solvents as well as to other conjugated polymers.

Results and discussion

Fabrication of oriented layers in a single step

In the first series of samples, we investigated the influence of blade speed when coating a CB solution containing P3HT and five times as much TCB ($m_{TCB}/m_{P3HT} = 5$). Interestingly, depending on the deposition parameters, two distinct regimes become apparent.[19] For low deposition speed, carrier solvent evaporation dominates the deposition behaviour. The polymer chains accumulate at the contact line and an already dried film is deposited behind the blade (evaporation regime). In this case TCB nucleation is confined to the blade edge, which results in cm^2-sized samples of uniaxially oriented polymers as shown in Fig. 1. For higher deposition speeds solvent evaporation cannot keep up and a liquid film forms on the substrate, which only dries after the blade has completed its sweep. This is usually called the Landau–Levich regime.[19] In this case, nucleation of TCB crystallites is not confined to the edge of the blade but instead occurs randomly across the whole sample. This results in large spherulites, similar to those obtained by spin coating[18] or by drop casting.

To illustrate the differences between the two deposition regimes, Fig. 1 shows polarized transmission photographs (top row) and cross-polarized optical micrographs. While the first two samples, deposited at a speed of 1 and 2 mm s^{-1}, show layers with a fibrillar texture of uniform orientation, the samples deposited at higher speed show an increasing number

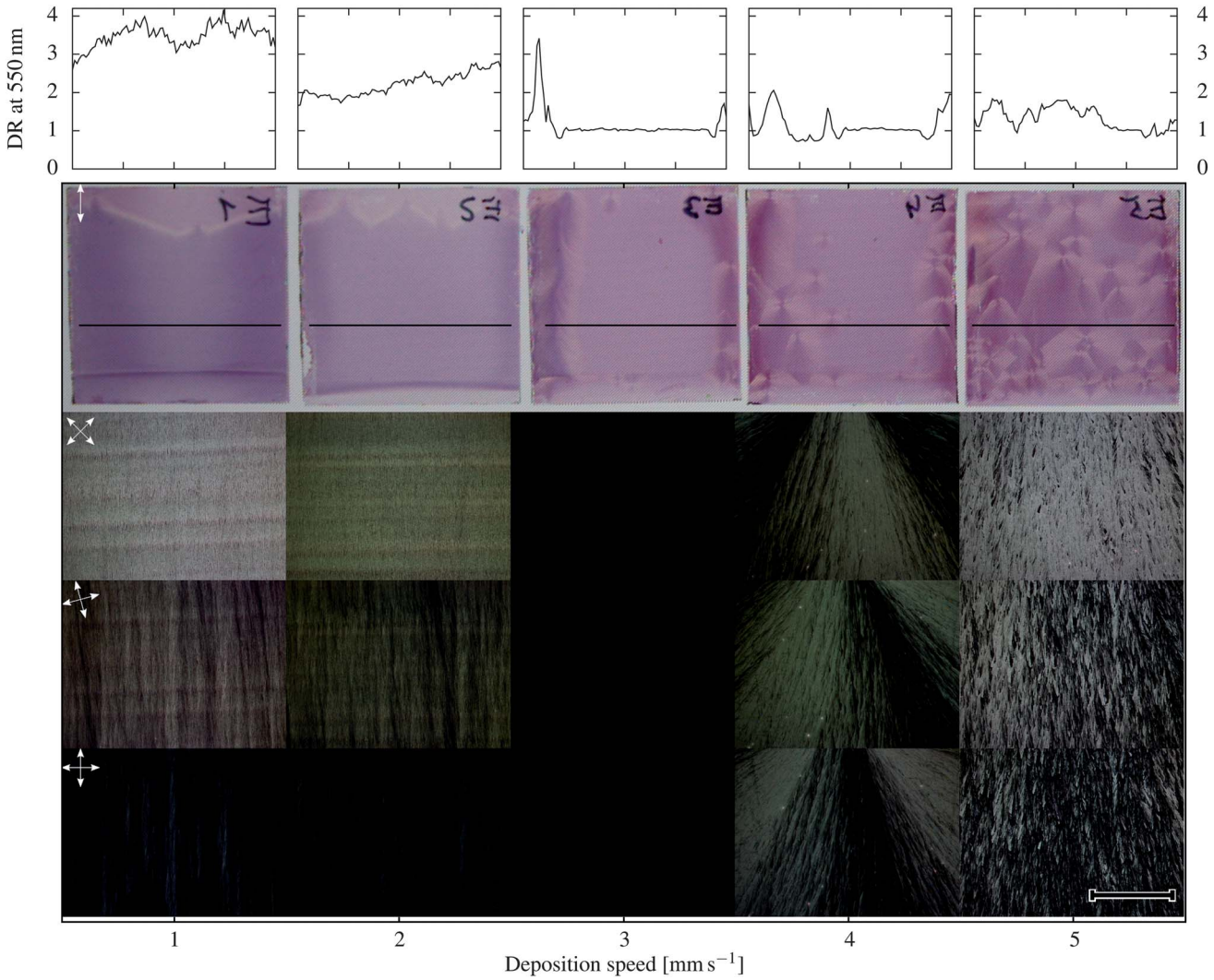

Fig. 1 Polarized transmission photographs and cross-polarized micrographs of samples deposited from a solution containing 20 mg ml^{-1} P3HT and $m_{TCB}/m_{P3HT} = 5$. From left to right, the deposition speed varies from 1 to 5 mm s^{-1}, encompassing both the evaporation and the Landau–Levich regimes, explained in detail in the text. Deposition direction was from top to bottom. Samples are 25 by 25 mm large. The length of the scale bar is 500 μm. The orientation of the polarizers is indicated by white arrows. An additional micrograph with crossed polarizers at 15° is provided to better illustrate the sample structure. The optical density was measured with light polarized vertically and horizontally every 250 μm with a spot diameter of 250 μm in a 24 mm long scan across the sample, as indicated by the black lines. The dichroic ratio was calculated at 550 nm.

of spherulites embedded in an otherwise isotropic layer. There is a clear transition between both regimes at a speed of around 3 mm s^{-1}, where no orientation is obtained, thus no light is transmitted through the crossed polarizers.

When depositing films by blade coating, increasing the speed typically increases the film thickness. Thicker films are also obtained by increasing the solute content of the solution that is coated. So in order to prove that the two regimes are related to a competition between evaporation and blade speed and not to a different film thickness, we prepared a new set of samples, doubling the polymer concentration while keeping the same ratio of TCB to P3HT ($m_{TCB}/m_{P3HT} = 5$). Reassuringly, we observed the same behaviour: uniaxial orientation for slow coating speed and spherulitic growth if the blade speed exceeds a critical value, as depicted in the ESI Fig. S1.†

In order to quantify the degree of orientation, we measured the transmittances $T_{||}$ for light polarized parallel and $T_{\perp}$ for light polarized perpendicular to the direction of the fibrillar texture of the polymer. From these we calculated the optical density $OD = -\log(T)$ and the dichroic ratio $DR = OD_{||}/OD_{\perp}$. Fig. 2 shows the result for a representative measurement. The DR at the maximum of absorption at 550 nm was 2.6, measured with a spot 3 mm in diameter. These values are only slightly smaller than values measured with a spot diameter of 250 μm, illustrating the uniform alignment.

Using the 250 μm spot, we measured transmittance maps across five samples fabricated at different blade speeds. The resulting DRs at 550 nm are plotted in Fig. 1. We observe a reasonably homogeneous DR across layers with fibrillar texture, with an apparent increase in the degree of orientation with decreasing blade speed, going from a DR of around 3.4 at 1 mm s^{-1} down to 2.3 at 2 mm s^{-1}. While the orientation within spherulites appears smaller, with the DR peaking at only 2, it should be noted that due to the angular distribution within a spherulite, an accurate value can only be measured with a probing spot much smaller than a spherulite.

It has to be pointed out that during deposition, excess solvent accumulates at the edges of the sample. This leads to an elevated TCB concentration at the sides and bottom of the substrate, which in turn leads to dichroism at the edges of otherwise completely isotropic samples, as is exemplified by the middle column in Fig. 1. These edge effects are confined to

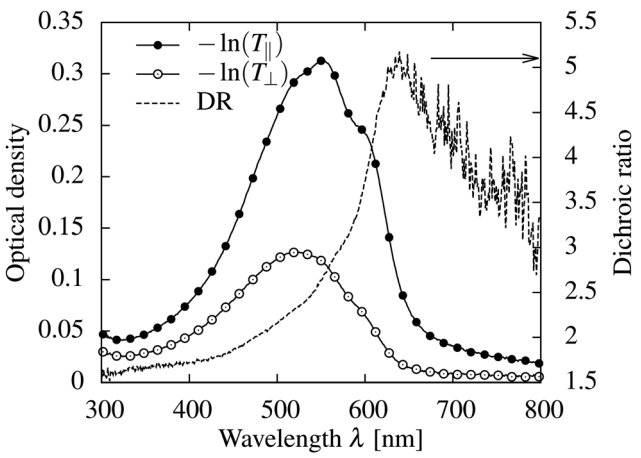

Fig. 2 Optical density for light polarized parallel (filled circles) and perpendicular (empty circles) to the direction of the fibrillar polymer features. The dichroic ratio (dashed line) at the absorption maximum of 550 nm is 2.6. The diameter of the spot was approximately 3 mm. It should be noted that the DR is expected to vanish for energies below the bandgap. The reported nonzero DR in this case is due to scattering.

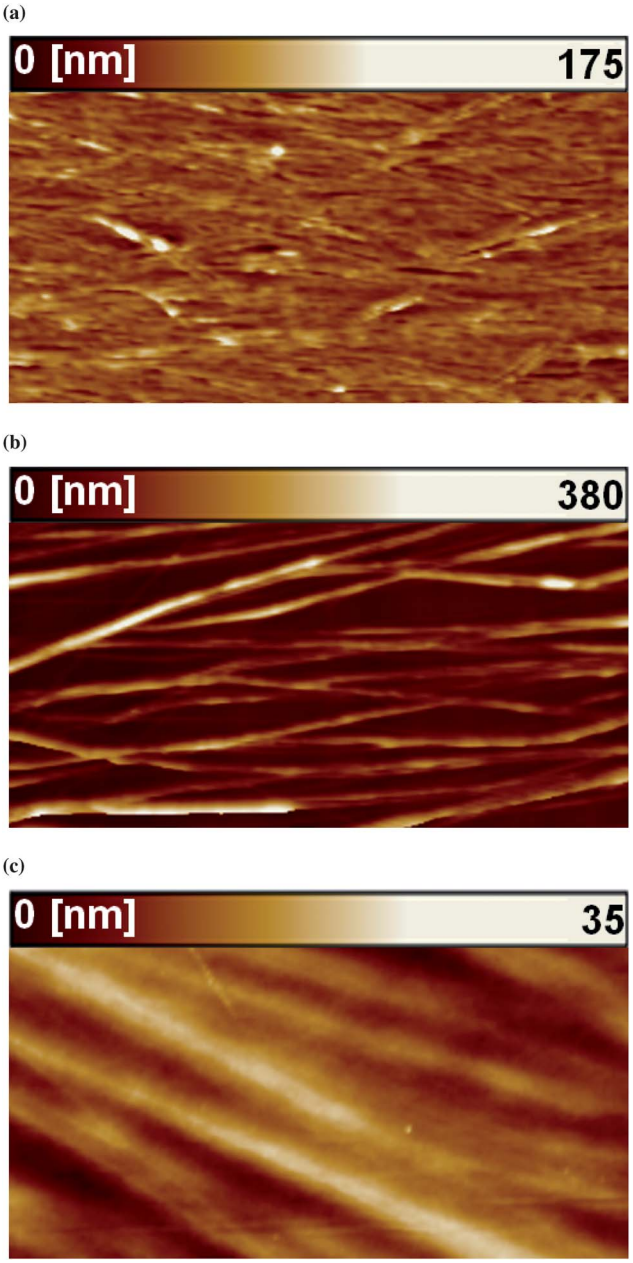

Fig. 3 AFM images of a 50 by 20 μm area, depicting the different types of layer textures. (a) shows a 90 nm thick spherulitic P3HT layer. (b) illustrates a P3HT layer with fibrillar texture, containing a significant amount of voids. (c) shows such a fibrillar P3HT layer after depositing PCBM from an orthogonal solvent on top. The roughness strongly decreases due to both rearranging of the P3HT structures and filling of the remaining voids with PCBM.

about 3 to 5 mm wide stripes and do not seem to depend on the substrate size, provided that a large enough substrate is used. Consequently, increasing the substrate size relatively decreases the affected area, and therefore does not impede a potential scaling up to large areas. Homogeneity of the whole sample could potentially be further increased by improving the control over the initial nucleation and ensuring sufficient circulation of the solution during deposition.[20]

In order to better understand the differences in the two main regimes, we characterized the sample structure by atomic force microscopy (AFM). The AFM images in Fig. 3 depict the differences between spherulitic layers and layers with a fibrillar texture. Aside from their degree and direction of orientation, they strongly differ in roughness. While spherulites show higher roughness than neat layers of P3HT, uniaxially oriented layers consist of fibrous structures that are even rougher. In fact, some of the latter type of samples consist of stacks of largely freestanding fibrous polymer structures separated by voids. It is still unclear if these voids reach all the way to the substrate, or if an unbroken polymer wetting layer is present on the substrate.

Next we study the effect of the ratio of TCB to P3HT. Fig. 4 shows a combinatorial array of samples deposited at varying blade speeds and from solutions containing different amounts of TCB. The corresponding cross-polarized micrographs are depicted in Fig. 5. Samples deposited from solutions with a ratio $m_{TCB}/m_{P3HT} < 3$ do not exhibit dichroism. Orientation is first observed for low speeds at a ratio of 3. This 2–3 cut-off mass ratio is similar to what we observed for samples deposited by spin coating.[18] Interestingly, the two regimes are observed for m_{TCB}/m_{P3HT} between 4 and 7 with the critical speed being

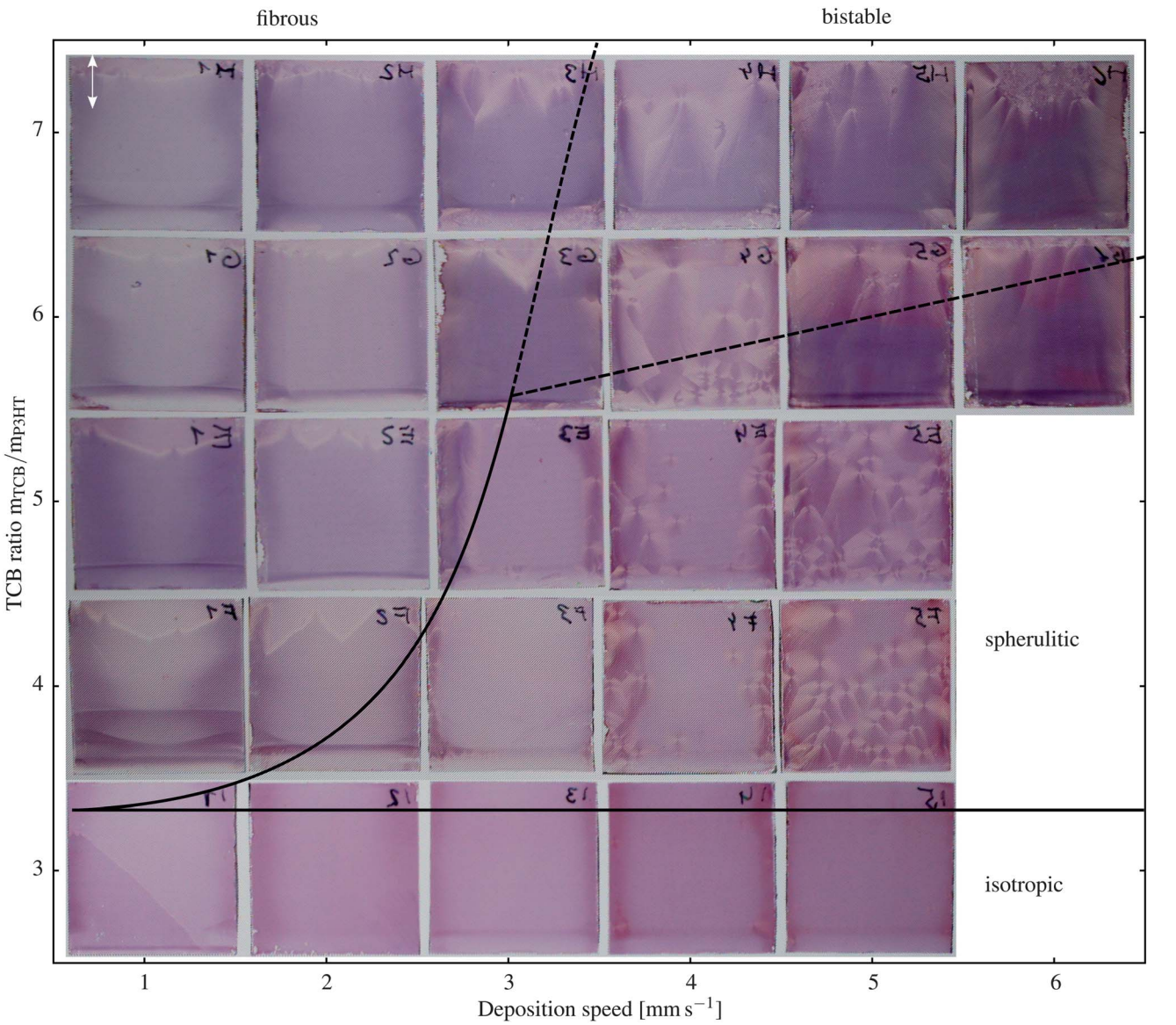

Fig. 4 Polarized transmission photographs of samples illustrating the effect of TCB concentration (*y*-axis) and deposition speed (*x*-axis). The orientation of the polarizer is indicated by the white arrow. Samples are 25 by 25 mm large. The overlaid boundaries indicate the qualitatively different types of samples that result from the different regimes.

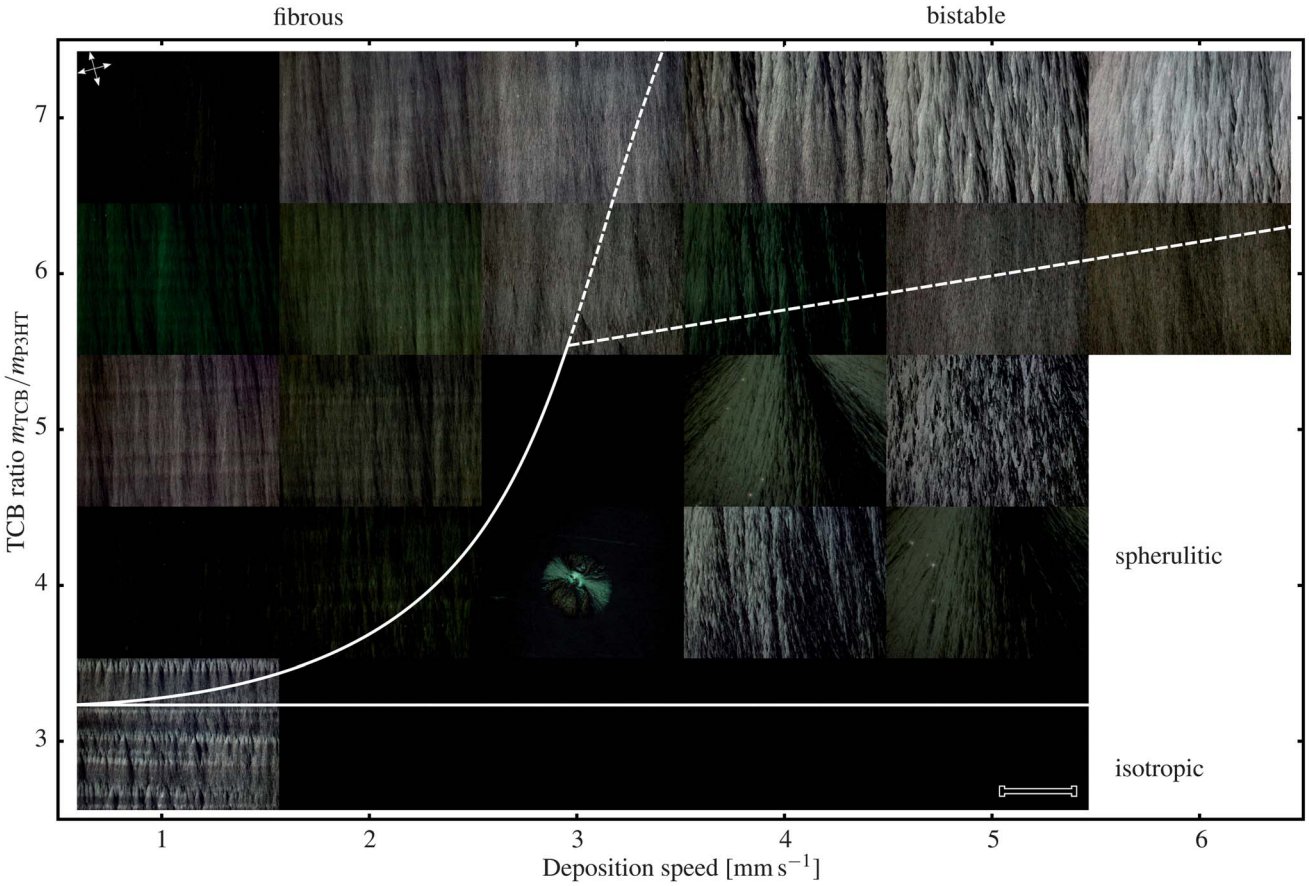

Fig. 5 Cross-polarized micrographs corresponding to samples from Fig. 4. The orientation of the crossed polarizers is indicated by white arrows. The length of the scale bar is 500 μm. Depositing from a solution with $m_{TCB}/m_{P3HT} \leq 3$ results in isotropic samples for all but the slowest deposition speeds. For $3 < m_{TCB}/m_{P3HT} < 6$ two types of samples can clearly be distinguished. Deposition speeds below 3 mm s^{-1} result in samples that have a fibrillar texture and exhibit uniaxial orientation on a macroscopic scale. High deposition speeds on the other hand lead to samples that are covered in spherulites. These two regimes adjoin at a deposition speed of 3 mm s^{-1}, where samples are mostly isotropic, interspersed with the odd spherulite. For $m_{TCB}/m_{P3HT} \geq 6$, the distinction is not as clear-cut, with samples deposited at higher speeds exhibiting both features. A more detailed summary of samples is provided in Fig. S2–S6.†

somewhere between 2 and 3 mm s^{-1}. At high mass ratios, the dry films exhibit a large fraction of voids left by the TCB upon sublimation. Combining large amounts of TCB with fast blade speed results in bistable drying during coating, with the appearance of fibrous and spherulitic areas within the same sample. Because of the statistical nature of the nucleation process, it is possible to obtain mutually exclusive areas of fibrillar texture and spherulites in direct contact. An example of this is shown in Fig. S7.†

Inspired by the useful phase diagram descriptions of mixtures, we have superimposed approximate regime frontiers on the pictures of the samples. Low m_{TCB}/m_{P3HT} leads to isotropic films. Intermediate values for m_{TCB}/m_{P3HT} result in oriented fibrous and spherulitic films for slow and fast blade speeds, respectively. Increasing m_{TCB}/m_{P3HT} to significantly larger values (data not shown) gradually increases the accumulation of the polymer, which results in increasingly porous films with ill-defined orientation.

Going further, we demonstrate that epitaxial crystallization of polymers from solution is not confined to a narrow range of materials that already show high inherent crystallinity, or fortuitously share matching lattice constants.

In Fig. 6(a) we show cross-polarized microscopy images of P3HT samples deposited from CB using naphthalene as a crystallizable additive, which provides the template for epitaxial growth. The naphthalene based samples exhibit many of the same features as those deposited from solutions containing TCB. While we did not observe uniaxial orientation on a large scale, the results still mirror those of TCB samples under imperfect conditions, specifically those that are deposited at a low TCB concentration. On the other hand, changing the polymer to one that does not crystallize easily, like PCPDTBT, still results in layers that exhibit dichroism. This is depicted in the cross-polarized micrographs in Fig. 6(b), which too resemble the P3HT/TCB samples.

These findings suggest that by selecting a suitable crystallizable solvent and adapting the processing conditions, a similar potential for uniaxial orientation and increase in crystallinity could be obtained for a range of polymers.[18]

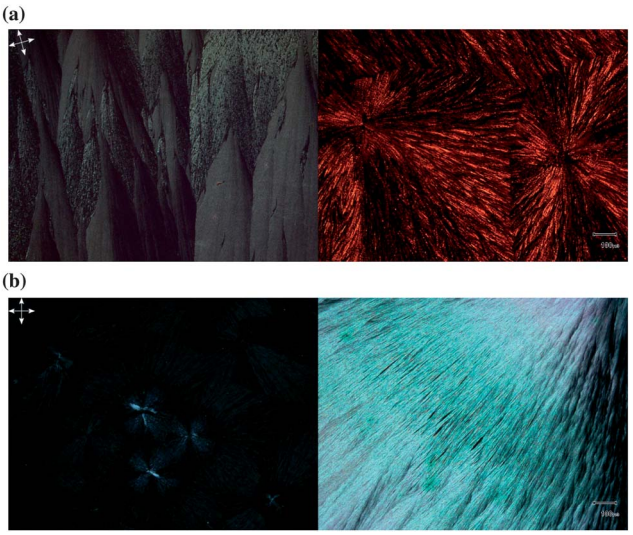

Fig. 6 Cross-polarized micrographs of samples fabricated using other combinations of crystallizable solvents and polymers. (a) shows P3HT samples deposited at 3 and 30 mm s^{-1} from a solution of CB with naphthalene as the crystallizable solvent, and (b) depicts PCPDTBT samples deposited at a speed of 3 and 5 mm s^{-1} from a solution of CB and TCB.

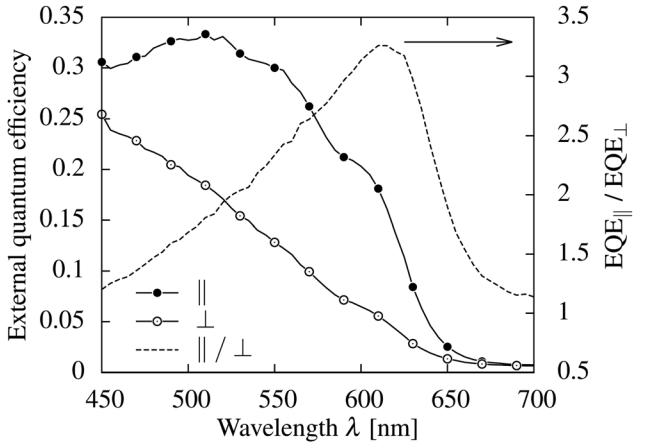

Fig. 7 EQE of a bilayer device with fibrillar P3HT layer measured under polarized illumination. Light is polarized parallel (filled circles) and perpendicular (empty circles) to the orientation of the fibrillar structures. The ratio $EQE_{||}/EQE_{\perp}$ is plotted as a dashed line.

Table 1 Average OPV device characteristics under polarized irradiance across four devices

Polarization	Irradiance [mW cm^{-2}]	J_{sc} [mA cm^{-2}]	V_{oc} [V]	FF [%]	η [%]
∥	44	1.1	0.56	47.2	0.67
⊥	44	0.72	0.52	43.2	0.38
Unpolarized	98	3.47	0.61	45.6	0.97

Polarization dependent devices

Recently, Zhu and co-workers demonstrated that OPV devices based on rubbed P3HT that are capped with a layer of [6,6]-phenyl-C61-butyric acid methyl ester (PCBM) show a photoresponse that depends on the polarization of light.[7] We set to investigate whether the method we have developed could be used to fabricate a similar device. First, we deposited a uniaxially aligned P3HT layer with fibrillar texture directly from solution onto substrates coated with ITO and PEDOT:PSS. Then, a cover layer of the acceptor material PCBM was deposited from dichloromethane, a non-solvent for P3HT, as reported previously.[15] The devices were completed by thermal evaporation of the Al cathode.

The external quantum efficiency (EQE) is plotted in Fig. 7 for light polarized parallel (filled circles) and perpendicular (empty circles) to the orientation direction. Reassuringly, polymer orientation is maintained through the different processing steps and results in a high anisotropic photovoltaic response. $EQE_{||}/EQE_{\perp}$ is about 2.3 for incident wavelengths around the absorption maximum of 550 nm. These results match the DR in absorption presented in Fig. 2, but they do not reach the values achieved with devices fabricated using an additional rubbing step, instead of the direct orientation during deposition.[7]

Table 1 summarizes the average performance of the four fabricated devices, while the *J–V*-characteristics are plotted in Fig. S8.† Both, Table 1 and Fig. 7 indicate that the devices presented here have a relatively low power conversion efficiency (η) compared to values of 3%, obtained for spin coated bilayer reference devices.

In order to understand this, we analysed the properties of the layers at the different stages of processing. Fig. 3 shows layers with a fibrillar texture before (b) and after (c) deposition of the PCBM top layer. Although P3HT was not dissolved during the PCBM deposition, the fibrillar structures have been displaced, leading to a total device thickness of 70 nm. For comparison, reference bilayers, that were spin-coated from a solution without added TCB, consist of a 90 nm thick P3HT layer and a 30 nm thick PCBM layer. In order to estimate the ratio between P3HT and PCBM in the fibrillar bilayers, we compared their absorption to that of the reference bilayers. The results plotted in Fig. S9† reveal that the absorption in the oriented devices is dominated by PCBM, indicating that they contain disproportionately less P3HT than the optimized reference devices. This could explain the unexpectedly large efficiency under unpolarized illumination. Moreover, photoluminescence (PL) measurements shown in Fig. S10† determined that the PL is not effectively quenched in fibrous P3HT layers after PCBM deposition. This stands in contrast to P3HT spherulites and layers of neat P3HT, where the deposition of a PCBM cover layer results in an efficient quenching of the PL. This suggests that the interdiffusion of P3HT and PCBM is very limited, most probably due to the expected high degree of crystallinity in the fibrous layers. This is likely to limit the charge transfer efficiency, and thus explains the relatively low overall device efficiencies.

Although a full device optimization goes beyond the scope of the present manuscript, the results are already promising with respect to the ability to fabricate oriented films and OPV devices with polarization dependent photoresponse. Indeed, Fig. 8 shows the dependence of the EQE at 550 nm on the polarization

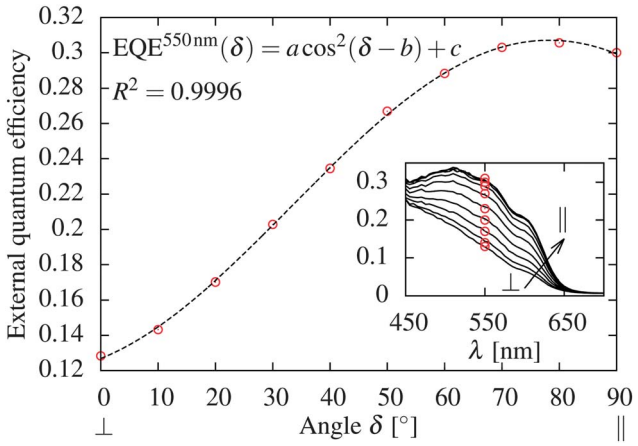

Fig. 8 Dependence of the EQE at 550 nm on the light polarization and fit of a Malus' law type of function to the data. The inset shows the EQE, measured in steps of 10°.

of the incoming light and demonstrates that this type of device could be employed as a simple, fully solid state polarization detector. The photoresponse follows a Malus' law type of dependence on polarization, as one would predict for a device whose photocurrent is proportional to the absorbed light. The maximum and minimum change of the EQE per degree, are 0.1880 and 0.0017 respectively. A conservative estimate of 1% for the measurement error in the absolute EQE value then translates to an angular resolution between 0.05 and 5.8°. We also measured the power conversion efficiency of the same device for polarization angles between 0 and 90°. The results are shown in Fig. S11† and agree well with those obtained for a single wavelength, demonstrating the polarization dependent photoresponse for non-monochromatic light.

Conclusions

In summary, we demonstrated a method to uniaxially align polymers directly from solution in a single step. This method is based on blade coating a solution containing the desired polymer and both the carrier solvent and a crystallizable solvent. We characterized the parameters that control the degree of orientation and found two distinct regimes, one useful for uniaxial orientation and another for spherulites. Using the acquired knowledge, we realized OPV devices with a polarization dependent photoresponse. Furthermore, we show that this method is widely applicable because it is not dependent on a single material combination. The technique developed in this work could help to simultaneously accomplish the so far disparate goals of highly crystalline, uniaxially oriented layers and the prospective strengths of organic electronics, ease of fabrication and price.

Experimental

Materials

Chemical structures of the materials used are given in Fig. S12.† The materials were used as received. 1,3,5-Trichlorobenzene (TCB, purity = 99%) and naphthalene (purity ≥ 99%) were bought from Sigma-Aldrich. Poly(3-hexylthiophene-2,5-diyl) (P3HT, $M_w = 97$ kg mol^{-1}, $M_w/M_n \approx 2.4$, regioregularity ≥ 90%) was obtained from Rieke Metals. For OPV devices, P3HT ($M_w =$ 40 kg mol^{-1}, $M_w/M_n \approx 2.0$, regioregularity ≥ 90%) was bought from Merck. Poly(3,4-ethylenedioxythiophene)-poly-(styrenesulfonate) (PEDOT:PSS, Clevios P VP Al 4083) was bought from H. C. Starck. Poly[2,6-(4,4-bis-(2-ethylhexyl)-4*H*-cyclopenta[2,1-*b*;3,4-*b*′]dithiophene)-*alt*-4,7(2,1,3-benzothiadiazole)] (PCPDTBT, $M_w = 25$ kg mol^{-1}, $M_w/M_n \approx 2.3$) was purchased from 1-Material. [6,6]-Phenyl C61 butyric acid methyl ester (PCBM) was purchased from Luminescence Technology Corp.

Preparation of optical samples

Cleaned 25 by 25 mm glass microscope slides were used as substrates. Samples were blade coated using a Zehntner ZAA-2300 coater and ZUA-2000 applicator from solutions containing 20 and 40 mg ml^{-1} P3HT in CB and $3 \leq m_{TCB}/m_{P3HT} \leq 7$. The blade height was set to 75 μm and the substrate temperature to 25 °C. The deposition speed varied between 1 and 6 mm s^{-1}. During deposition, the evaporation of the solvent was accelerated by applying a horizontal flow of nitrogen of 4 l min^{-1} in the deposition direction across the sample. Due to practical limitations of the deposition speed, this measure proved necessary in order to be able to reach the evaporation regime. The effect of this flow of nitrogen is pictured in Fig. S13.† While there is a significant difference between samples fabricated without and with an applied flow, increasing the flow further does not qualitatively change the result, since the contact line already moves as fast as the blade. Attempts at reaching the evaporation regime by the somewhat simpler and more intuitive way of heating did not prove fruitful. This is owed to the large difference between the boiling point of CB ($T_B^{CB} = 132$ °C) and the melting point of TCB ($T_M^{TCB} \approx 62$ °C). Instead, depositing at increased temperature strongly decreases the nucleation density of TCB, resulting in samples that are isotropic, until initial nucleation occurs, as documented in ESI Fig. S14.† Even after changing to a low-boiling solvent like chloroform ($T_B^{CHCl_3} = 61$ °C), the evaporation regime was only reached with the help of a flow of nitrogen. Samples were stored in a mild vacuum overnight to remove potential remaining solvent.

OPV device preparation

ITO coated glass substrates were sonicated in acetone, detergent and isopropanol, before being dried in isopropanol vapor and UV–ozone treated. An approximately 40 nm thick layer of PEDOT:PSS was spin coated at 4000 rpm for 30 s and subsequently annealed at 100 °C for 10 min. The P3HT layer was blade coated at a speed of 2 mm s^{-1} from a CB solution containing 40 mg ml^{-1} P3HT and $m_{TCB}/m_{P3HT} = 5$. PCBM was spin coated for 10 s at 4000 rpm from a 10 mg ml^{-1} solution in dichloromethane. After thermally evaporating a 100 nm aluminium cathode, samples were annealed for 10 min at 120 °C. The device active area was defined to 2 mm^2.

Measurements

Polarized photometry was carried out using a GES5E ellipsometer from Semilab. Polarized optical micrographs were taken using an Olympus BX51 optical microscope and a DP20 microscope digital camera. Atomic force microscopy images were taken using a Keyence Nanoscale Hybrid Microscope VN-8000. Device characteristics were measured using a Keithley 2400 Source meter under simulated AMG 1.5G illumination of an 150 W Xenon Oriel Research Arc Source. In the case of polarized illumination, a polarizer was placed in the light path.

Acknowledgements

The authors thank Christian Müller (Chalmers University of Technology, Sweden) for his help at the beginning of this study and for continuous fruitful discussions. We are grateful to the Ministerio de Economía y Competitividad for funding through projects PLE2009-0086, CSD2010-00044 (Consolider NANOTHERM) and MAT2012-37776.

References

1 H. Sirringhaus, R. J. Wilson, R. H. Friend, M. Inbasekaran, W. Wu, E. P. Woo, M. Grell and D. D. C. Bradley, *Appl. Phys. Lett.*, 2000, **77**, 406.
2 T. Kreouzis, D. Poplavskyy, S. Tuladhar, M. Campoy-Quiles, J. Nelson, A. Campbell and D. D. C. Bradley, *Phys. Rev. B: Condens. Matter Mater. Phys.*, 2006, **73**, 235201.
3 H.-M. Liem, P. Etchegoin, K. Whitehead and D. D. C. Bradley, *Adv. Funct. Mater.*, 2003, **13**, 66–72.
4 M. Campoy-Quiles, P. G. Etchegoin and D. D. C. Bradley, *Phys. Rev. B: Condens. Matter Mater. Phys.*, 2005, **72**, 045209.
5 K. Vandewal, K. Tvingstedt and O. Inganäs, *Phys. Rev. B: Condens. Matter Mater. Phys.*, 2012, **86**, 035212.
6 M. Grell and D. D. C. Bradley, *Adv. Mater.*, 1997, 798–802.
7 R. Zhu, A. Kumar and Y. Yang, *Adv. Mater.*, 2011, **23**, 4193–4198.
8 C. Müller, M. Garriga and M. Campoy-Quiles, *Appl. Phys. Lett.*, 2012, **101**, 171907.
9 B. O'Connor, R. J. Kline, B. R. Conrad, L. J. Richter, D. J. Gundlach, M. F. Toney and D. M. DeLongchamp, *Adv. Funct. Mater.*, 2011, **21**, 3697–3705.
10 P. Dyreklev and G. Gustafsson, *Solid State Commun.*, 1992, **82**, 317–320.
11 P. Dyreklev, M. Berggren, O. Inganäs, M. R. Andersson, O. Wennerström and T. Hjertberg, *Adv. Mater.*, 1995, **7**, 43–45.
12 Z. Zheng, K.-H. Yim, M. S. M. Saifullah, M. E. Welland, R. H. Friend, J.-S. Kim and W. T. S. Huck, *Nano Lett.*, 2007, **7**, 987–992.
13 J. C. Wittmann and P. Smith, *Nature*, 1991, **352**, 414–417.
14 M. Hamaguchi and K. Yoshino, *Appl. Phys. Lett.*, 1995, **67**, 3381–3383.
15 V. Vohra, G. Arrighetti, L. Barba, K. Higashimine, W. Porzio and H. Murata, *J. Phys. Chem. Lett.*, 2012, **3**, 1820–1823.
16 M. Brinkmann and J. C. Wittmann, *Adv. Mater.*, 2006, **18**, 860–863.
17 J. C. Wittmann and B. Lotz, *Prog. Polym. Sci.*, 1990, **15**, 909–948.
18 C. Müller, M. Aghamohammadi, S. Himmelberger, P. Sonar, M. Garriga, A. Salleo and M. Campoy-Quiles, *Adv. Funct. Mater.*, 2013, **23**, 2368–2377.
19 M. Le Berre, Y. Chen and D. Baigl, *Langmuir*, 2009, **25**, 2554–2557.
20 Y. Diao, B. C.-K. Tee, G. Giri, J. Xu, D. H. Kim, H. A. Becerril, R. M. Stoltenberg, T. H. Lee, G. Xue, S. C. B. Mannsfeld and Z. Bao, *Nat. Mater.*, 2013, **12**, 665–671.

